

# The Proper Motion of the Local Group Galaxy IC 10

A. Brunthaler<sup>1</sup>, M.J. Reid<sup>2</sup>, H. Falcke<sup>3,4</sup>, C. Henkel<sup>1</sup>, and K.M. Menten<sup>1</sup>

<sup>1</sup> Max-Planck-Institut für Radioastronomie, Auf dem Hügel 69, 53121 Bonn, Germany

<sup>2</sup> Harvard-Smithsonian Center for Astrophysics, 60 Garden Street, Cambridge, MA 02138, USA

<sup>3</sup> ASTRON, Postbus 2, 7990 AA Dwingeloo, the Netherlands

<sup>4</sup> Department of Astrophysics, Radboud Universiteit Nijmegen, Postbus 9010, 6500 GL Nijmegen, The Netherlands

Received; accepted

**Abstract.** We have measured the proper motion of the Local Group galaxy IC 10 with the Very Long Baseline Array by measuring the position of an H<sub>2</sub>O maser relative to two background quasars over 4.3 years. After correction for the rotation of the Milky Way and IC 10, we obtain a motion of  $-39 \pm 9 \mu\text{as yr}^{-1}$  toward the East and  $31 \pm 8 \mu\text{as yr}^{-1}$  toward the North. This corresponds to a total space velocity of  $215 \pm 42 \text{ km s}^{-1}$  relative to the Milky Way for an assumed distance of  $660 \pm 66 \text{ kpc}$ . Assuming that IC 10 and M33, for which also a proper motion measurement exists, are bound to M31, we calculate a lower limit for the mass of M31 of  $7.5 \times 10^{11} M_{\odot}$ .

**Key words.** Astrometry – Galaxies: Local Group – Galaxies: individual: IC 10 – Galaxies: kinematics and dynamics – Dark Matter

## 1. Introduction

### 1.1. Proper Motions in the Local Group

Proper motion measurements of Local Group galaxies are important for our understanding of the dynamics and evolution of the Local Group. Presently, measurements of extragalactic proper motions by optical telescopes are limited to the most nearby companions of the Milky Way, i.e. the LMC (Jones, Klemola, & Lin 1994; Kallivayalil et al. 2006; Pedreros, Costa, & Méndez 2006), the SMC (Kallivayalil, van der Marel, & Alcock 2006), the Sculptor dwarf spheroidal galaxy (dShp) (Schweitzer et al. 1995; Piatek et al. 2006), the Canis Major dwarf galaxy (Dinescu et al. 2005b), the Ursa Minor dSph (Piatek et al. 2005), the Sagittarius dSph (Dinescu et al. 2005a), the Fornax dSph (Piatek et al. 2002; Dinescu et al. 2004), and the Carina dSph (Piatek et al. 2003). These galaxies are all closer than 150 kpc and show motions between 0.2 and a few milliarcseconds (mas) per year. More distant galaxies, such as galaxies in the Andromeda subgroup at distances of  $\sim 800 \text{ kpc}$ , have smaller angular motions, which are currently not measurable with optical telescopes.

On the other hand, Brunthaler et al. (2005) measured the proper motions of two groups of water masers on opposite sides of M33 at radio frequencies with the NRAO<sup>1</sup> Very Long Baseline Array (VLBA). A comparison of the relative proper

motion between the two groups of masers and their expected motions from the known rotation curve and inclination of M33 led to a determination of a “rotational parallax” ( $730 \pm 168 \text{ kiloparsec}$ ) for this galaxy. This distance is consistent with recent Cepheid and tip of the red giant branch estimates (Lee et al. 2002; McConnachie et al. 2005) and earlier distance estimates using the internal motions of water masers in the IC 133 region (Greenhill et al. 1993; Argon et al. 2004).

Since the proper motion measurements were made relative to a distant extragalactic background source, the proper motion of M33 itself could also be determined. This measured proper motion of M33 is a first important step toward a kinematical model of the Local Group and was used to constrain the proper motion and dark matter content of the Andromeda Galaxy M31 (Loeb et al. 2005).

Water masers in Local Group galaxies have also been found toward the Magellanic Clouds (e.g. Scalise & Braz 1981) and IC 10 (e.g. Henkel, Wouterloot, & Bally 1986). Other Local Group galaxies were searched, but no additional water masers have been detected (see Brunthaler et al. 2006 and references therein). In this paper we report on VLBA observations of the maser in IC 10 to measure its motion.

### 1.2. IC 10

The extragalactic nature of IC 10 was first recognized by Mayall (1935). Hubble (1936) proposed that it was likely a member of the Local Group and described it as “one of the most curious objects in the sky”. However, observations of IC 10 have been always difficult because of the low Galactic

Send offprint requests to: brunthal@mpifr-bonn.mpg.de

<sup>1</sup> The National Radio Astronomy Observatory is operated by Associated Universities, Inc., under a cooperative agreement with the National Science Foundation.

**Table 1.** Details of the observations: Observing date, observation length  $t_{obs}$ , beam size  $\theta$  and position angle  $PA$ .

Epoch	Date	$t_{obs}$ [h]	$\theta$ [mas]	$PA$ [°]
I	2001/02/09	10	0.53×0.33	-15
I	2001/03/28	10	0.55×0.36	-18
I	2001/04/12	10	0.63×0.37	-5
II	2002/01/12	10	0.59×0.35	-19
II	2002/01/17	10	0.64×0.32	-22
III	2002/10/01	10	0.68×0.38	-12
III	2002/10/11	10	0.61×0.34	-5
IV	2003/12/12	12	0.52×0.33	-15
IV	2004/01/10	12	0.50×0.33	-23
V	2004/08/23	12	0.60×0.51	-2
V	2004/09/18	12	0.54×0.35	-17
VI	2005/06/01	12	0.60×0.50	-11
VI	2005/06/07	12	0.56×0.39	-6

latitude of 3°. IC 10 has been classified as an IrIV galaxy (e.g. van den Bergh 1999), but Richer et al. (2001) argue that it has more properties of a blue compact dwarf galaxy. It is also the nearest galaxy hosting a small starburst, evidenced by its large number of Wolf-Rayet stars (Massey, Armandroff, & Conti 1992) and the discovery of 144 H II regions (Hodge & Lee 1990). Observations of HI with the Westerbork Synthesis Radio Telescope by Shostak & Skillman (1989) revealed that IC 10 has a regularly rotating disk surrounded by a counter-rotating outer distribution of gas.

The distance to IC 10 is subject to controversy because of difficulties caused by its low Galactic latitude. Early estimates claim a distance of 1–1.5 Mpc (Roberts 1962) and 3 Mpc (Bottinelli, Gouguenheim, & Heidmann 1972, Sandage & Tammann 1974). Huchtmeier (1979) argued for a closer distance of 1 Mpc. The most recent determination from multi-wavelength observations of Cepheid variables obtained a distance of  $660 \pm 66$  kpc to IC 10 (Sakai, Madore, & Freedman 1999), which we adopt throughout this paper.

IC 10 hosts two known H<sub>2</sub>O masers, IC 10-SE and IC 10-NW (Becker et al. 1993). The strong SE-component was first detected by Henkel, Wouterloot, & Bally (1986) and the whole spectrum of IC 10 showed strong variability since its discovery with flux densities between less than 1 Jy (Becker et al. 1993) and a flare with a (single dish) flux density of 125 Jy (Baan & Haschick 1994). Even intraday variability has been reported by Argon et al. (1994), but the strong component at  $v_{LSR} \approx -324$  km s<sup>-1</sup> has been persistent until now.

## 2. Observations and Data Reduction

We observed the usually brightest maser in IC 10-SE with the VLBA thirteen times between February 2001 and June 2005. The observations are grouped into six epochs, each comprising two closely spaced observations, except the first epoch with three observations, to enable assessment of overall accuracy and systematic errors (Table 1).

We observed in four 8 MHz bands in dual circular polarization. The 128 spectral channels in each band yielded a channel

spacing of 62.5 kHz, equivalent to 0.84 km s<sup>-1</sup>, and covered a velocity range of 107 km s<sup>-1</sup>. The observations involved rapid switching between the phase-calibrator VCS1 J0027+5958 from the VLBA Calibrator Survey (Beasley et al. 2002), which is a compact background source with continuum emission, and the target sources IC 10 and NVSS J002108+591132. NVSS J002108+591132 is a radio continuum source from the NRAO VLA Sky Survey (NVSS) (Condon et al. 1998) and is located only 8 arcminutes from the maser in IC 10. It was also detected in X-rays (Wang, Whitaker, & Williams 2005) and is most likely also a background quasar. The redshifts of VCS1 J0027+5958 and NVSS J002108+591132 are not known. We switched sources every 30 seconds in the sequence VCS1 J0027+5958 – IC 10 – VCS1 J0027+5958 – NVSS J002108+591132 – VCS1 J0027+5958 and achieved on-source integration times of  $\sim 22$  seconds. The background sources were assumed to be stationary on the sky. Since the phase-calibrator is separated by only 1° on the sky from the target sources, one can obtain precise angular separation measurements.

From the second epoch on, we included *geodetic-like* observations where we observed for 45 minutes 10–15 strong radio sources ( $> 200$  mJy) with accurate positions ( $< 1$  mas) at different elevations to estimate an atmospheric zenith delay error in the VLBA calibrator model (see Reid & Brunthaler 2004 and Brunthaler, Reid, & Falcke 2005 for a discussion). In the second and third epoch we used two blocks of these geodetic observations before and after the phase-referencing observations. From the fourth epoch on, we included a third geodetic block in the middle of the observation.

The data were edited and calibrated using standard techniques in the Astronomical Image Processing System (AIPS). A-priori amplitude calibration was applied using system temperature measurements and standard gain curves. Zenith delay corrections were performed based on the results of the geodetic-like observations. Data from the St. Croix station were flagged due to high phase noise in all observations. The maser in IC 10 and NVSS J002108+591132 were imaged in AIPS. All detected maser features and NVSS J002108+591132 were unresolved and fit by single elliptical Gaussian components.

## 3. Results

### 3.1. Spatial Structure

In the first epoch, maser emission could be detected in 21 channels spread over  $\approx 23$  km s<sup>-1</sup>. The spatial distribution of the masers on 2001 March 28 can be seen in Fig. 1. It is similar to the distribution in earlier VLBI observations of IC 10 by Argon et al. (1994). The strongest component at a LSR velocity of  $\approx -324$  km s<sup>-1</sup> is separated by  $\approx 10$  mas or (projected) 6600 AU from the weaker components. This suggests that the emission is associated with a single object if the maser emission is similar to H<sub>2</sub>O maser emission in Galactic star forming regions like W3(OH), W49 or Sgr B2 (e.g. Reid et al. 1995, Walker et al. 1977 and Kobayashi et al. 1989 respectively). The weaker maser components form an apparent ring-like structure with a projected size of  $\approx 1.6$  mas or 1060 AU.

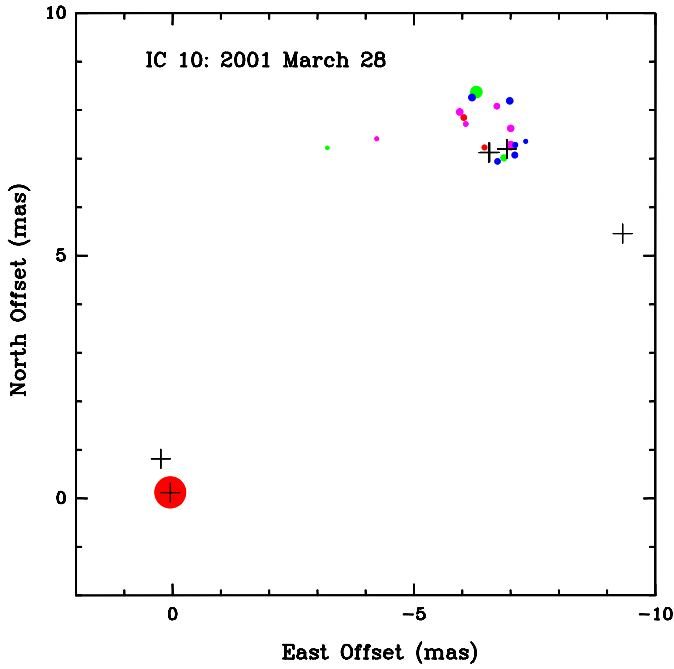


**Fig. 1.** Composite map of the H<sub>2</sub>O masers in IC 10 from 2001 March 28. The area of each circle is proportional to the flux density of the respective component. The colors denote different LSR radial velocities with  $> -327$  km s<sup>-1</sup> (red),  $-327$  to  $-330$  km s<sup>-1</sup> (magenta),  $-330$  to  $-338$  km s<sup>-1</sup> (green), and  $< -338$  km s<sup>-1</sup> (blue). The crosses mark the positions of the maser emission detected by Argon et al. (1994). The positions were aligned on the strongest maser component in the south-east.

### 3.2. Variability

The correlated flux density of the strong feature at  $-324$  km s<sup>-1</sup> LSR velocity increased from 1.0 to 1.5 Jy between the first two VLBA observations of the first epoch. The weaker components are also very variable and they can appear or disappear between observations. In the observations of the second epoch, the flux density of the strongest component was  $\sim 1.1$  Jy and some of the weaker components disappeared. In the third epoch, we detected only the strong component with a flux density of  $\sim 0.7$  Jy while the weak ring-like structure was not detected anymore. In the later epochs, the flux density of the remaining component dropped to  $\sim 0.2$  Jy, 0.12 Jy, and 0.07 Jy in the fourth, fifth, and sixth epoch, respectively.

### 3.3. Observed Motions

The position offsets of the strongest maser feature in IC 10 are shown in Fig. 2. The uncertainties in the observations of the first epoch are larger than the others, because no geodetic-like observations were done to compensate the zenith delay errors. A rectilinear motion was fit to the data and yielded a value of  $-2 \pm 6$   $\mu$ as yr<sup>-1</sup> toward the East and  $20 \pm 6$   $\mu$ as yr<sup>-1</sup> toward the North.

The position offsets of NVSS J002108+591132 are shown in Fig. 3. A rectilinear motion was fit to the data and yielded a motion of  $-10 \pm 3$   $\mu$ as yr<sup>-1</sup> toward the East and  $-5 \pm 5$   $\mu$ as yr<sup>-1</sup> toward the North. Hence, NVSS J002108+591132 shows a

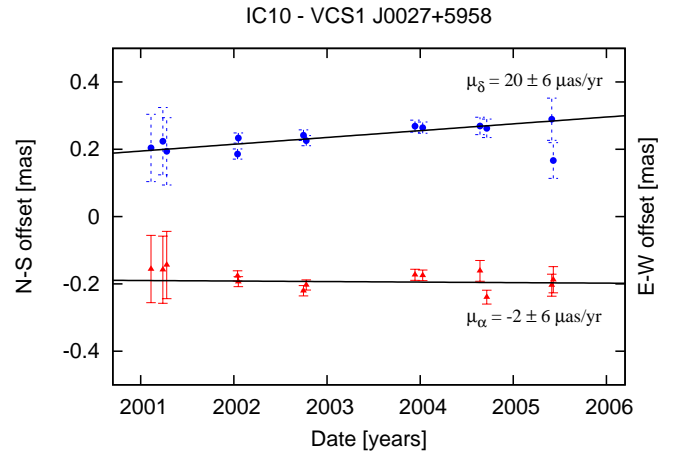


**Fig. 2.** The position of the maser in IC 10 relative to the phase-reference source VCS1 J0027+5958 in East-West (red triangles) and North-South (blue circles). The lines show a variance weighted linear fit to the data points.

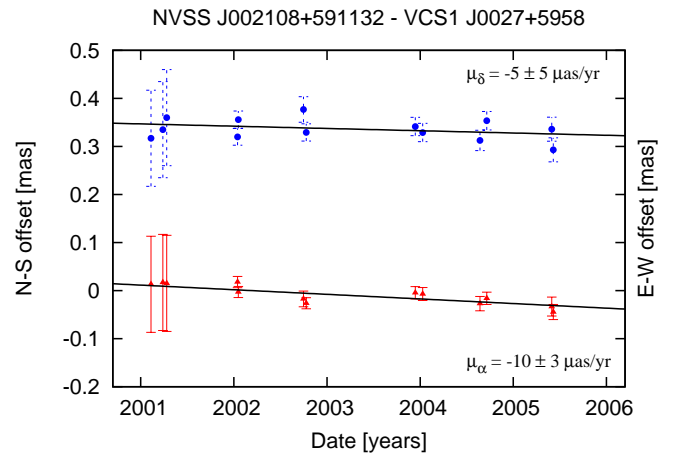


**Fig. 3.** The position of NVSS J002108+591132 relative to the phase-reference source VCS1 J0027+5958 in East-West (red triangles) and North-South (blue circles). The lines show a variance weighted linear fit to the data points.

small but potentially significant motion in right ascension. The apparent motion of NVSS J002108+591132 could be caused by unknown systematic errors.

The phase calibrator VCS1 J0027+5958 may have unresolved structure, e.g. a core-jet structure. The observed image of the source is the convolution of the source structure and the synthesized beam of the VLBA. Flux density variations of the individual components could move the position of the observed image by a fraction of the beam size. Since the phase calibrator is assumed to be stationary, this would shift the positions of all target sources by the same amount.

The observed motion of NVSS J002108+591132 could also be caused by some errors in the geometry of the correlator model (i.e. antenna positions, earth orientation parameters). These errors would be similar for closely spaced observations, but different for observations separated by several months. The angular separation between IC 10 and NVSS

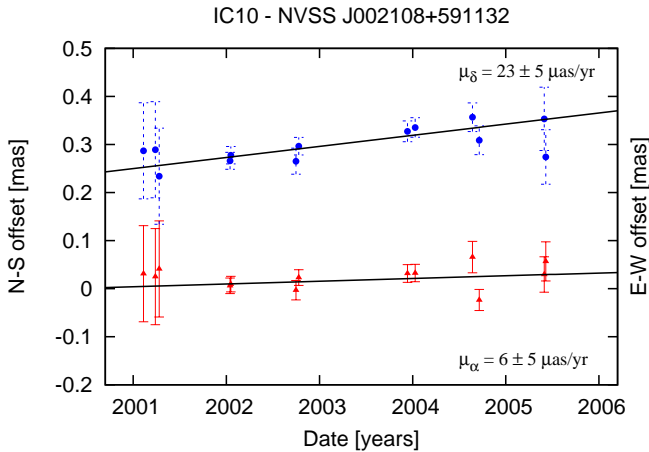


**Fig. 4.** The position of the strongest maser feature in IC 10 relative to NVSS J002108+591132 in East-West (red triangles) and North-South (blue circles). The lines show a variance weighted linear fit to the data points.

J002108+591132 ( $8'$ ) is much smaller than the separation between IC 10 and VCS1 J0027+5958 ( $1^\circ$ ), and the position shift induced by geometric errors would be similar for IC 10 and NVSS J002108+591132.

In both cases, the motion of the maser in IC 10 relative to NVSS J002108+591132 would be a better estimate of the proper motion of IC 10. However, it cannot be ruled out that the apparent motion of NVSS J002108+591132 is caused by an unresolved core-jet structure in NVSS J002108+591132 itself. Since strong sources are expected to show more jet-structure than weak sources, amplitude variations of VCS1 J0027+5958 (70–290 mJy) are larger than those in NVSS J002108+591132 (6–11 mJy), and the angular separation between IC 10 and NVSS J002108+591132 is much smaller than the separation between IC 10 and VCS1 J0027+5958, we consider NVSS J002108+591132 as the better astrometric reference source. Fig. 4 shows the position of the strongest maser component in IC 10 relative to NVSS J002108+591132. A rectilinear motion was fit to the data and yielded a motion of  $6 \pm 5 \mu\text{as yr}^{-1}$  toward the East and  $23 \pm 5 \mu\text{as yr}^{-1}$  toward the North and we will adopt these values for the proper motion of the maser.

## 4. Discussion

### 4.1. Space Motion of IC 10

The measured proper motion  $\tilde{\mathbf{v}}_{prop}$  of the maser in IC 10 can be decomposed into a sum of several components, relative to a frame at rest at the center of the Milky Way:

$$\tilde{\mathbf{v}}_{prop} = \mathbf{v}_{rot} + \mathbf{v}_{pec} + \mathbf{v}_{\odot} + \mathbf{v}_{IC10} \quad (1)$$

Here  $\mathbf{v}_{rot}$  is the motion of the masers due to the internal galactic rotation in IC 10,  $\mathbf{v}_{pec}$  is the peculiar motion of the masers relative to circular galactic rotation and  $\mathbf{v}_{\odot}$  is the apparent motion of IC 10 caused by the rotation of the Sun about the Galactic Center. The last contribution  $\mathbf{v}_{IC10}$  is the true proper motion of the galaxy IC 10.

The  $\text{H}_2\text{O}$  masers in IC 10 are located within a massive HI cloud in the central disk. If one assumes that the masers are rotating with the disk, one can calculate its expected proper motion. Shostak & Skillman (1989) measure an inclination of  $45^\circ$  from the ellipticity of its HI distribution. The masers are 33 arcseconds (106 pc) east and 99 arcseconds (317 pc) south of the kinematic center. Unfortunately no position angle of the major axis was given. Wilcots & Miller (1998) used higher resolution VLA observations of the HI content of IC 10 to fit a tilted ring model to the velocity field of the disk of IC 10. This model has a separate rotation speed, inclination and position angle for each ring. They find a highly inclined disk in the inner 110 arcseconds with a position angle of  $\approx 75^\circ$  and a rotational velocity of  $\approx 30 \text{ km s}^{-1}$ . The position of the kinematic center of their tilted ring model was not given. If one combines the kinematic center of Shostak & Skillman (1989) with the inclination and position angle of Wilcots & Miller (1998), one gets an expected transverse motion for the maser ( $\mathbf{v}_{rot}$ ) of 26 and 11  $\text{km s}^{-1}$  toward the East and North, respectively.

If one calculates the expected motion for different realistic scenarios (i.e. changing the kinematic center by  $\pm 20$  arcseconds, and the inclination and the position angle of the major axis by  $\pm 20^\circ$ ), one gets always transverse motions between 20–30  $\text{km s}^{-1}$  toward the East and 5–15  $\text{km s}^{-1}$  toward the North. The deviation of the motion of the masers from the galactic rotation is unknown. The radial velocity of the CO gas at the position of the maser in IC 10 is about  $-330 \text{ km s}^{-1}$  (Becker 1990), which is close to the radial velocity of the maser. In our Galaxy peculiar motions of star forming regions can be 20  $\text{km s}^{-1}$  as seen in W3(OH) (Xu et al. 2006; Hachisuka et al. 2006). Hence, to be conservative, we adopt values of  $25 \pm 20$  and  $10 \pm 20 \text{ km s}^{-1}$  toward the East and North, respectively. This translates to  $\dot{\alpha}_{rot} = 8 \pm 6$  and  $\dot{\delta}_{rot} = 3 \pm 6 \mu\text{as yr}^{-1}$  at a distance of  $660 \pm 60 \text{ kpc}$ .

The rotation of the Sun about the Galactic Center causes an apparent motion of IC 10. The motion of the Sun can be decomposed into a circular motion of the local standard of rest (LSR) and the peculiar motion of the Sun. The peculiar motion of the Sun has been determined from Hipparcos data by Dehnen & Binney (1998) to be in  $\text{km s}^{-1}$   $U_0 = 10.00 \pm 0.36$  (radially inwards),  $V_0 = 5.25 \pm 0.62$  (in the direction of Galactic rotation) and  $W_0 = 7.17 \pm 0.38$  (vertically upwards). VLBI measurements of the proper motion of SgrA\*, the compact radio source at the Galactic Center, yield a motion of  $6.379 \pm 0.026 \text{ mas yr}^{-1}$  along the Galactic plane (Reid et al. 1999; Reid & Brunthaler 2004). Combined with a recent geometric distance estimate of the Galactic Center of  $7.62 \pm 0.32 \text{ kpc}$  (Eisenhauer et al. 2005), one gets a circular velocity of  $225 \pm 10 \text{ km s}^{-1}$  for the LSR.

This motion of the Sun causes an apparent proper motion of  $38 \pm 4 \mu\text{as yr}^{-1}$  in Galactic longitude and  $-6 \pm 1 \mu\text{as yr}^{-1}$  in Galactic latitude (for a distance of 660 kpc and Galactic coordinates of IC 10 of  $l = 118.96^\circ$ ,  $b = -3.32^\circ$ ). Converted to equatorial coordinates, one gets  $\dot{\alpha}_{\odot} = 37 \pm 4 \mu\text{as yr}^{-1}$  and  $\dot{\delta}_{\odot} = -11 \pm 1 \mu\text{as yr}^{-1}$ .

The true proper motion of IC 10 is then given by

$$\dot{\alpha}_{IC10} = \dot{\alpha}_{prop} - \dot{\alpha}_{rot} - \dot{\alpha}_{\odot}$$

$$\begin{aligned}
&= (6 (\pm 5) - 8 (\pm 6) - 37 (\pm 4)) \mu\text{as yr}^{-1} \\
&= -39 \pm 9 \mu\text{as yr}^{-1} = -122 \pm 31 \text{ km s}^{-1}
\end{aligned}$$

and

$$\begin{aligned}
\dot{\delta}_{IC\ 10} &= \dot{\delta}_{prop} - \dot{\delta}_{rot} - \dot{\delta}_{\odot} \\
&= (23 (\pm 5) - 3 (\pm 6) + 11 (\pm 1)) \mu\text{as yr}^{-1} \\
&= 31 \pm 8 \mu\text{as yr}^{-1} = 97 \pm 27 \text{ km s}^{-1}
\end{aligned}$$

The measured systematic heliocentric velocity of IC 10 ( $-344 \pm 3 \text{ km s}^{-1}$ , de Vaucouleurs et al. 1991) is the sum of the radial motion of IC 10 toward the Sun and the component of the solar motion about the Galactic Center toward IC 10 which is  $-196 \pm 10 \text{ km s}^{-1}$ . Hence IC 10 is moving with  $148 \pm 10 \text{ km s}^{-1}$  toward the Sun.

The proper motion and the radial velocity combined give the three-dimensional space velocity of IC 10. The total velocity is  $215 \pm 42 \text{ km s}^{-1}$  relative to the Milky Way. This velocity vector is shown in the schematic view of the Local Group in Fig. 5. Here, we used Cartesian coordinates, where the Sun is located at the origin and the Galactic Center is located at  $(x,y,z)=(7.62,0,0)$  (see Appendix A for details).

#### 4.2. Local Group Dynamics and Mass of M31

If IC 10 or M33 are bound to M31, then the velocity of the two galaxies relative to M31 must be smaller than the escape velocity and one can deduce a lower limit on the mass of M31:

$$M_{M31} > \frac{v_{rel}^2 R}{2G}. \quad (3)$$

A relative velocity of  $147 \text{ km s}^{-1}$  – for a zero tangential motion of M31 – and a distance of 262 kpc between IC 10 and M31, gives a lower limit of  $6.6 \times 10^{11} M_{\odot}$ . One can repeat this calculation for any tangential motion of M31. The results are shown in Fig. 6 (top). The lowest value of  $0.7 \times 10^{11} M_{\odot}$  is found for a tangential motion of M31 of  $-130 \text{ km s}^{-1}$  toward the East and  $35 \text{ km s}^{-1}$  toward the North.

For a relative motion of  $230 \text{ km s}^{-1}$  between M33 and M31 – again for a zero tangential motion of M31 – and a distance of 202 kpc, one gets a lower limit of  $1.2 \times 10^{12} M_{\odot}$  (Brunthaler et al. 2005). Fig. 6 (top) shows also the lower limit of the mass of M31 for different tangential motions of M31 if M33 is bound to M31. The lowest value is  $4 \times 10^{11} M_{\odot}$  for a tangential motion of M31 of  $-115 \text{ km s}^{-1}$  toward the East and  $160 \text{ km s}^{-1}$  toward the North.

Loeb et al. (2005) find that proper motions of M31 in negative right ascension and positive declination would have lead to close interactions between M31 and M33 in the past. These proper motions of M31 can be ruled out, since the stellar disk of M33 does not show any signs of strong interactions. Loeb et al. (2005) used a total mass of M31 of  $3.4 \times 10^{12} M_{\odot}$  in their simulations. Although simulations with lower masses of M31 yield weaker interactions, motions in negative right ascension and positive declination are still ruled out.

Thus, we can rule out these regions in Fig. 6. This results in a lower limit of  $7.5 \times 10^{11} M_{\odot}$  for M31 and agrees with a

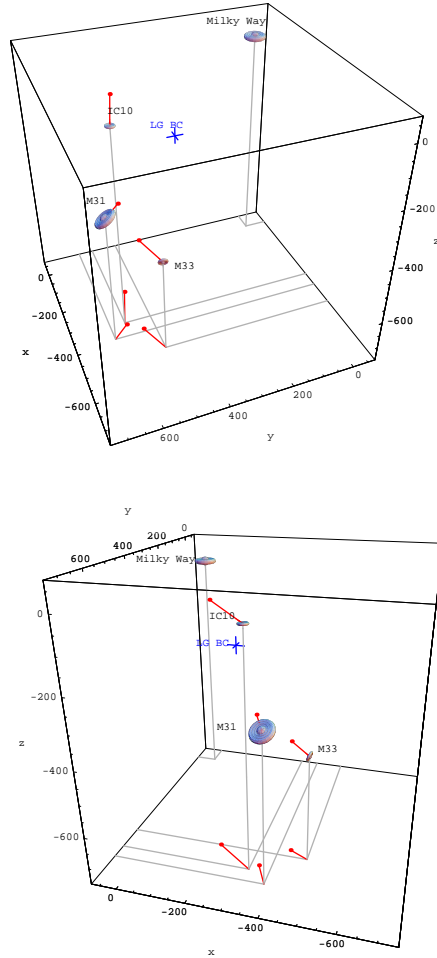


**Fig. 5.** Schematic view of the Local Group from two viewing angles with the space velocity of IC 10 and M33 (the latter taken from Brunthaler et al. 2005) and the radial velocity of Andromeda relative to the Milky Way. The blue cross marks the position of the Local Group Barycenter (LG BC) according to van den Bergh (1999).

recent estimate of  $12.3^{+18}_{-6} \times 10^{11} M_{\odot}$  derived from the three-dimensional positions and radial velocities of its satellite galaxies (Evans & Wilkinson 2000).

## 5. Summary

We have presented astrometric VLBA observations of the  $\text{H}_2\text{O}$  maser in the Local Group galaxy IC 10. We detected a ring-like structure in one epoch with a projected diameter of  $\sim 1060 \text{ AU}$ . We measured the proper motion of the maser relative to two background quasars. Correcting for the internal rotation of IC 10 and the rotation of the Milky Way this measurement yields a proper motion of  $-39 \pm 9 \mu\text{as yr}^{-1}$  toward the East and  $31 \pm 8 \mu\text{as yr}^{-1}$  toward the North, which corresponds to a total space velocity of  $215 \pm 42 \text{ km s}^{-1}$  for IC 10 relative to the Milky Way. If IC 10 and M33 are bound to M31, one can calculate a lower limit of the mass of M31 of  $7.5 \times 10^{11} M_{\odot}$ .

*Acknowledgements.* This research was supported by the DFG Priority Programme 1177.

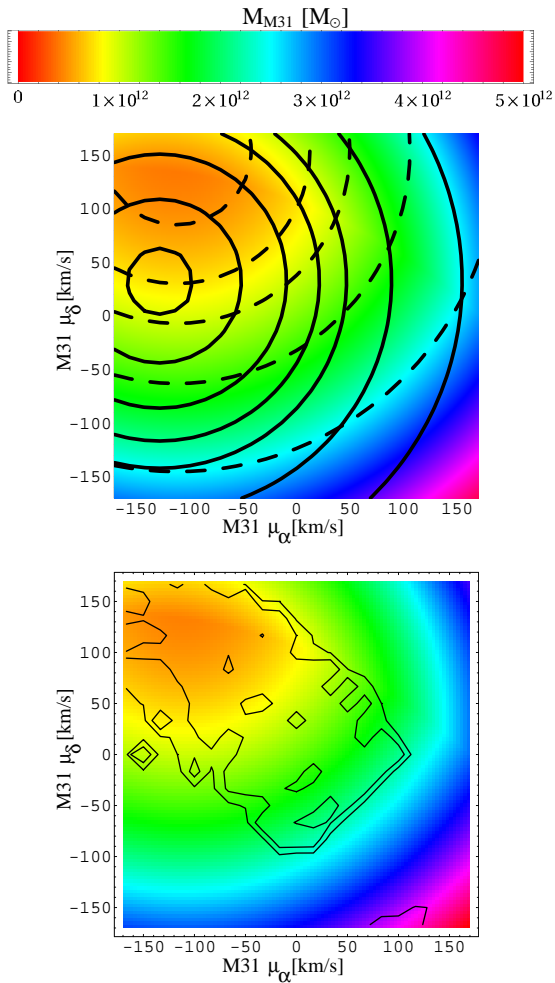


**Fig. 6. Top:** Lower limit on the mass of M31 for different tangential motions of M31 assuming that M33 (dashed) or IC 10 (solid) are bound to M31. The lower limits are  $(4, 5, 7.5, 10, 15, 25) \times 10^{11} M_{\odot}$  for M33, and  $(0.7, 1, 2.5, 5, 7.5, 10, 15, 25) \times 10^{11} M_{\odot}$  for IC 10, rising from inside. The colour scale indicates the maximum of both values. **Bottom:** The colour scale is the same as above and gives the lower limit on the mass of M31. The contours show ranges of proper motions that would have lead to a large amount of stars stripped from the disk of M33 through interactions with M31 or the Milky Way in the past. The contours delineate 20% and 50% of the total number of stars stripped (Loeb et al. 2005). These regions can be excluded, since the stellar disk of M33 shows no signs of such interactions.

## References

- Argon A. L., Greenhill L. J., Moran J. M., et al., 1994, *ApJ*, 422, 586  
 Argon A. L., Greenhill L. J., Moran J. M., et al., 2004, *ApJ*, 615, 702  
 Baan W. A., Haschick A., 1994, *ApJ*, 424, L33  
 Beasley A. J., Gordon D., Peck A. B., et al., 2002, *ApJS*, 141, 13  
 Becker R., 1990, Ph.D. Thesis  
 Becker R., Henkel C., Wilson T. L., Wouterloot J. G. A., 1993, *A&A*, 268, 483  
 Bottinelli L., Gouguenheim L., Heidmann J., 1972, *A&A*, 18, 121  
 Brunthaler A., Henkel C., de Blok W. J. G., et al., 2006, *A&A*, 457, 109  
 Brunthaler A., Reid M. J., Falcke H., 2005, *Atmosphere-Corrected Phase-Referencing*, in ASP Conf. Ser. 340: Future Directions in High Resolution Astronomy, p. 455  
 Brunthaler A., Reid M. J., Falcke H., Greenhill L. J., Henkel C., 2005, *Science*, 307, 1440  
 Condon J. J., Cotton W. D., Greisen E. W., et al., 1998, *AJ*, 115, 1693  
 de Vaucouleurs G., de Vaucouleurs A., Corwin H. G., et al., 1991, *Third Reference Catalogue of Bright Galaxies. Volume 1-3, XII*, 2069 pp. 7 figs.. Springer-Verlag Berlin Heidelberg New York  
 Dehnen W., Binney J. J., 1998, *MNRAS*, 298, 387  
 Dinescu D. I., Girard T. M., van Altena W. F., López C. E., 2005a, *ApJ*, 618, L25  
 Dinescu D. I., Keeney B. A., Majewski S. R., Girard T. M., 2004, *AJ*, 128, 687  
 Dinescu D. I., Martínez-Delgado D., Girard T. M., et al., 2005b, *ApJ*, 631, L49  
 Eisenhauer F., Genzel R., Alexander T., et al., 2005, *ApJ*, 628, 246  
 Evans N. W., Wilkinson M. I., 2000, *MNRAS*, 316, 929  
 Greenhill L. J., Moran J. M., Reid M. J., Menten K. M., Hirabayashi H., 1993, *ApJ*, 406, 482  
 Hachisuka K., Brunthaler A., Menten M. K., et al., 2006, *ApJ*, 645, 337  
 Henkel C., Wouterloot J. G. A., Bally J., 1986, *A&A*, 155, 193  
 Hodge P., Lee M. G., 1990, *PASP*, 102, 26  
 Hubble E. P., 1936, Yale University Press  
 Huchtmeier W. K., 1979, *A&A*, 75, 170  
 Jones B. F., Klemola A. R., Lin D. N. C., 1994, *AJ*, 107, 1333  
 Kallivayalil N., van der Marel R. P., Alcock C., 2006, *ArXiv Astrophysics e-prints*  
 Kallivayalil N., van der Marel R. P., Alcock C., et al., 2006, *ApJ*, 638, 772  
 Kobayashi H., Ishiguro M., Chikada Y., et al., 1989, *PASJ*, 41, 141  
 Lee M. G., Kim M., Sarajedini A., Geisler D., Gieren W., 2002, *ApJ*, 565, 959  
 Loeb A., Reid M. J., Brunthaler A., Falcke H., 2005, *ApJ*, 633, 894  
 Massey P., Armandroff T. E., Conti P. S., 1992, *AJ*, 103, 1159  
 Mayall N. U., 1935, *PASP*, 47, 317  
 McConnachie A. W., Irwin M. J., Ferguson A. M. N., et al., 2005, *MNRAS*, 356, 979  
 Pedreros M. H., Costa E., Méndez R. A., 2006, *AJ*, 131, 1461  
 Piatek S., Pryor C., Bristow P., et al., 2005, *AJ*, 130, 95  
 Piatek S., Pryor C., Bristow P., et al., 2006, *AJ*, 131, 1445  
 Piatek S., Pryor C., Olszewski E. W., et al., 2002, *AJ*, 124, 3198  
 Piatek S., Pryor C., Olszewski E. W., et al., 2003, *AJ*, 126, 2346  
 Reid M. J., Argon A. L., Masson C. R., Menten K. M., Moran J. M., 1995, *ApJ*, 443, 238  
 Reid M. J., Brunthaler A., 2004, *ApJ*, 616, 872  
 Reid M. J., Readhead A. C. S., Vermeulen R. C., Treuhaft R. N., 1999, *ApJ*, 524, 816  
 Richer M. G., Bullejos A., Borissova J., et al., 2001, *A&A*, 370, 34  
 Roberts M. S., 1962, *AJ*, 67, 431  
 Sakai S., Madore B. F., Freedman W. L., 1999, *ApJ*, 511, 671  
 Sandage A., Tammann G. A., 1974, *ApJ*, 194, 559  
 Scalise E., Braz M. A., 1981, *Nat.*, 290, 36  
 Schweitzer A. E., Cudworth K. M., Majewski S. R., Suntzeff N. B., 1995, *AJ*, 110, 2747  
 Shostak G. S., Skillman E. D., 1989, *A&A*, 214, 33  
 van den Bergh S., 1999, *A&A Rev.*, 9, 273  
 Walker R. C., Burke B. F., Johnston K. J., Spencer J. H., 1977, *ApJ*, 211, L135  
 Wang Q. D., Whitaker K. E., Williams R., 2005, *MNRAS*, 362, 1065  
 Wilcots E. M., Miller B. W., 1998, *AJ*, 116, 2363  
 Xu Y., Reid M. J., Zheng X. W., Menten K. M., 2006, *Science*, 311, 54

## Appendix A: Coordinate Transformations

We define a Cartesian coordinate system where the Sun is located at the origin. To convert from Galactic to Cartesian coordinates, we used

$$\begin{pmatrix} x \\ y \\ z \end{pmatrix} = \begin{pmatrix} R \cos l \cos b \\ R \sin l \cos b \\ R \sin b \end{pmatrix}, \quad (\text{A.1})$$

where  $R$  is the distance,  $l$  is the Galactic Longitude, and  $b$  is the Galactic Latitude.

To convert the proper motions in right ascension ( $\dot{\alpha}$ ) and declination ( $\dot{\delta}$ ) into proper motions in Galactic Longitude ( $\dot{l}$ ) and Galactic Latitude ( $\dot{b}$ ), we used

$$\begin{pmatrix} \dot{l} \\ \dot{b} \end{pmatrix} = \begin{pmatrix} \cos \theta & \sin \theta \\ -\sin \theta & \cos \theta \end{pmatrix} \begin{pmatrix} \dot{\alpha} \\ \dot{\delta} \end{pmatrix}, \quad (\text{A.2})$$

where  $\theta$  is the required rotation angle at the position of the source (i.e.  $\theta_{IC\ 10} = -6.94^\circ$ ,  $\theta_{M33} = -348.95^\circ$ ,  $\theta_{M31} = -2.74^\circ$ ).

To compute the velocities in Cartesian coordinates, we constructed for each source three orthogonal vectors  $\mathbf{e}_r$ ,  $\mathbf{e}_l$ , and  $\mathbf{e}_b$  given by

$$\mathbf{e}_r = \begin{pmatrix} x \\ y \\ z \end{pmatrix}; \quad \mathbf{e}_l = \begin{pmatrix} \frac{y}{x} \\ -1 \\ 0 \end{pmatrix}; \quad \mathbf{e}_b = \mathbf{e}_r \times \mathbf{e}_l. \quad (\text{A.3})$$

These vectors can be normalized to give three orthogonal unit vectors  $\hat{\mathbf{e}}_r$ ,  $\hat{\mathbf{e}}_l$ , and  $\hat{\mathbf{e}}_b$ . Then the total velocity  $\mathbf{v}_{\text{tot}}$  of an object with proper motions  $\dot{l}$ ,  $\dot{b}$ , and the radial velocity  $v_{\text{rad}}$  is

$$\mathbf{v}_{\text{tot}} = \dot{l} \hat{\mathbf{e}}_l + \dot{b} \hat{\mathbf{e}}_b + v_{\text{rad}} \hat{\mathbf{e}}_r. \quad (\text{A.4})$$